The Role of Atlantic Basin Geometry in Meridional Overturning Circulation

SARAH RAGEN,[a] KYLE C. ARMOUR,[a,b] LUANNE THOMPSON,[a] ANDREW SHAO,[c] AND DAVID DARR[a]

[a] *School of Oceanography, University of Washington, Seattle, Washington*
[b] *Department of Atmospheric Sciences, University of Washington, Seattle, Washington*
[c] *Canadian Centre for Climate Modelling and Analysis, Environment and Climate Change Canada, Victoria, British Columbia, Canada*

(Manuscript received 18 February 2021, in final form 24 December 2021)

ABSTRACT: We present idealized simulations to explore how the shape of eastern and western continental boundaries along the Atlantic Ocean influences the Atlantic meridional overturning circulation (AMOC). We use a state-of-the art ocean–sea ice model (MOM6 and SIS2) with idealized, zonally symmetric surface forcing and a range of idealized continental configurations with a large, Pacific-like basin and a small, Atlantic-like basin. We perform simulations with five coastline geometries along the Atlantic-like basin that range from coastlines that are straight to coastlines that are shaped like the coasts of the American and African continents. Changing the Atlantic basin coastline shape influences AMOC strength in a manner distinct from simply increasing basin width: widening the basin while maintaining straight coastlines leads to a 10-Sv (1 Sv $\equiv 10^6$ m^3 s^{-1}) increase in AMOC strength, whereas widening the basin with the geometry of the American and African continents leads to a 6-Sv increase in AMOC strength, despite both cases representing the same average basin-width increase relative to a control case. The structure of AMOC changes are different between these two cases as well: a more realistic basin geometry results in a shoaled AMOC while widening the basin with straight boundaries deepens AMOC. We test the influence of the shape of the both boundaries independently and find that AMOC is more sensitive to the American coastline while the African coastline impacts the abyssal circulation. We also find that AMOC strength and depth scales well with basin-scale meridional density difference, even with different Atlantic basin geometries, illuminating a robust physical link between AMOC and the North Atlantic western boundary density gradient.

KEYWORDS: Atlantic Ocean; Meridional overturning circulation; General circulation models; Idealized models; Ocean models

1. Introduction

The global ocean circulation exhibits several large-scale hemispheric asymmetries, including, perhaps most notably, the deep-water formation and ventilation down to 2000 m at northern high latitudes that is present in the North Atlantic Ocean but is absent in the North Pacific Ocean (Ganachaud and Wunsch 2000; Lumpkin and Speer 2007; Talley 2008; Buckley and Marshall 2016; Ferreira et al. 2018). The deep-water formation in the North Atlantic is linked to the large-scale overturning circulation that crosses the equator in the Atlantic. In the high-latitude North Atlantic, shallow warm, salty water is cooled at the surface and sinks, forming North Atlantic Deep Water, which flows southward at depth. This water upwells in the Southern Ocean, drawn up by westerlies [for reviews, see Marshall and Speer (2012) and Buckley and Marshall (2016)]. Some of the upwelled water flows northward across the equator in the Atlantic, sustaining the Atlantic meridional overturning circulation (AMOC). In contrast, the Pacific is characterized by an absence of deep ventilation, a weak abyssal overturning circulation, and shallow wind-driven subtropical cells (Ganachaud and Wunsch 2000).

Northward heat transport occurs at all latitudes in the Atlantic basin and peaks at about 1.2 PW near 20°, over one-half of which is accomplished by AMOC, defined as the zonally integrated meridional currents in the Atlantic (Trenberth and Caron 2001; Talley 2003; Ferrari and Ferreira 2011). This northward heat transport is partially responsible for the warmer average temperature of the Northern Hemisphere as compared with the Southern Hemisphere (Vellinga and Wood 2002; Kuhlbrodt et al. 2007) and for the peak in zonal-mean rainfall residing north of the equator (Frierson et al. 2013; Marshall et al. 2014). It also influences regional climates of North America and Europe (Sutton and Hodson 2005; Kaspi and Schneider 2011; Woollings et al. 2012). Thus, AMOC plays a key role in setting up hemispheric asymmetries in climate. AMOC strength is linked to the warming hole in the North Atlantic (Drijfhout et al. 2012) as well as to the depth of ocean heat storage and the global transient response to climate change (Winton et al. 2013; Kostov et al. 2014). Moreover, AMOC is also important for the distribution of carbon and nutrients in the ocean (Sabine et al. 2004; Watson et al. 2015; Smethie and Fine 2001) that are linked to the geography of marine ecosystems in the Atlantic (Schmittner et al. 2005).

Despite the prominent role that large-scale meridional overturning plays in the global climate system, consensus has yet to emerge on its controlling mechanisms or the reason for its localization to the Atlantic basin (Ferreira et al. 2018). The deep ventilation in the Atlantic is linked to the higher salinity of the Atlantic basin (Warren 1983), explanations for which fall into two broad categories: atmosphere-driven salinity asymmetries due to differences in net surface freshwater fluxes (precipitation

Denotes content that is immediately available upon publication as open access.

Corresponding author: Sarah Ragen, sragen@uw.edu

DOI: 10.1175/JPO-D-21-0036.1

minus evaporation) and ocean-driven salinity asymmetries due to circulation and salt transport. Smaller atmospheric freshwater input is thought to account for about half the difference in the mean sea surface salinity between the Atlantic and the Pacific (Ferreira et al. 2018). The narrower width of the Atlantic relative to the rainfall fetch for water evaporated over both ocean basins leads to greater precipitation over the Pacific than over the Atlantic (Ferreira et al. 2010). The Atlantic basin also has more evaporation per unit area than the Pacific basin (Warren 1983; Nilsson et al. 2013). Ocean circulation may also play a role in the higher salinity, and thus localization of AMOC, in the Atlantic basin. These studies have predominantly explored the sensitivity to basin width (zonal extent) and basin length (meridional extent) using idealized continents with straight coastlines to separate a narrower, Atlantic-like basin from a wider Pacific-like basin. Such a configuration leads to a saltier Atlantic-like basin, which in turn leads to the localization of meridional overturning to the Atlantic, both in coupled (Ferreira et al. 2010; Nilsson et al. 2013) and in ocean-only simulations using zonally uniform atmospheric forcing (Cessi and Jones 2017; Jones and Cessi 2017). Moreover, the wider the basin, the smaller the meridional gradient in evaporation minus precipitation must be to shut off northern high-latitude convection, thus making a narrower basin more likely to support deep convection than a wider basin (Youngs et al. 2020).

Changing the width of the Atlantic-like basin in simulations with idealized forcing and geometry has been shown to change the strength of AMOC. Ocean-only simulations using zonally uniform atmospheric forcing suggest that widening the Atlantic-like basin leads to a weaker AMOC (Jones and Cessi 2017; Youngs et al. 2020). Jones and Cessi (2017) hypothesize a mechanism for this result: because gyre transport scales with basin width (Sverdrup 1947), narrower basins have weaker southward flowing subpolar western boundary currents than wider basins do. There is also a northward component of the western boundary velocity associated with the meridional overturning circulation, the strength of which is independent of basin width. In a narrower basin, the wind-driven subpolar western boundary component is weaker than the northward AMOC-associated velocities, allowing salty subtropical water to flow north into the subpolar gyre, which acts to weaken stratification in the northern subpolar region, allowing deep ventilation in the narrow basin.

A different theoretical argument suggests that widening the basin could lead to greater meridional ocean transport since wider basins have a larger effective isopycnal diffusivity associated with wind-driven gyre and mesoscale eddy transport (Wang et al. 1995; Rose and Marshall 2009; Nilsson et al. 2021). Thus, in a wider basin, the northward eddy-induced transport of heat and salt across the boundary between the subtropical and subpolar gyre causes competing effects on the high-latitude surface density by allowing relatively warm, salty water to flow farther north than in a narrow basin. If the surface temperatures are low in the northern sinking region, the salinity effects can dominate the temperature effects, increasing the density of the surface water and increasing the overturning strength.

Additionally, the meridional extent of the continents favors salt transport into the Atlantic basin from the Indian Ocean, increasing the salinity of the Atlantic over the Indo-Pacific and thus contributing to a preference for deep convection in the Atlantic (Reid 1961; Sijp and England 2009; Nilsson et al. 2013; Cessi and Jones 2017).

As reviewed above, theories exist that predict both an increase and a decrease in AMOC strength in response to a widening of the Atlantic-like basin. It is also reasonable to expect that the shape of the Atlantic as a function of latitude could impact the structure and strength of AMOC through interactions with the Sverdrup gyre transport at different latitudes. That is, the structure and strength of AMOC could depend on basin width at different latitudes—the shape of the basin. Additionally, widening the ocean basin by a constant number of degrees longitude (as in Jones and Cessi 2017) results in a greater increase in width in the tropics as compared with higher-latitude regions, thus increasing the Sverdrup transport in the subtropical and subpolar regions unequally. This raises a key question: how does the AMOC depend on the shape of the Atlantic basin coastlines?

Here, we explore this question using a state-of-the-art ocean–sea ice model with idealized, zonally symmetric surface forcing under a range of idealized continental configurations with different Atlantic coastlines. Following previous studies, we examine the ocean circulation within an ocean-only simulation that has a large Pacific-like basin and a small Atlantic-like basin. However, we go beyond these previous studies by exploring five different coastline geometries that impart different shapes to the Atlantic basin (Fig. 1). Using these simulations, we examine how Atlantic basin geometry influences the strength and structure of AMOC. While sensitivity of AMOC to the shape of the coastlines in our simulations is observed, no clear mechanisms emerge that link the two. In the later half the study, we thus evaluate a scaling for AMOC based on the meridional density gradient along the western boundary and use this scaling to understand the causes of the AMOC changes.

2. Methods

This section describes the physical configuration of the model components, the atmospheric forcing, and the five different continental configurations used (Fig. 1).

a. Model description

We use the most recent version of the Modular Ocean Model (MOM6) (Adcroft et al. 2019), an open-development project originally developed by the Geophysical Fluid Dynamics Laboratory (GFDL). The model is configured with a 2° horizontal resolution, 31 vertical levels using a geopotential, or z^* coordinate, and a uniformly spaced, bipolar grid. There are land caps at both poles from 70° to 90° to avoid the convergence of longitude lines in the ocean. The ocean is uniformly 5000 m deep with purely vertical sidewall boundaries. Our MOM6 configuration uses the Wright equation of state to calculate seawater density (Wright 1997). The model does not form Antarctic Bottom Water in

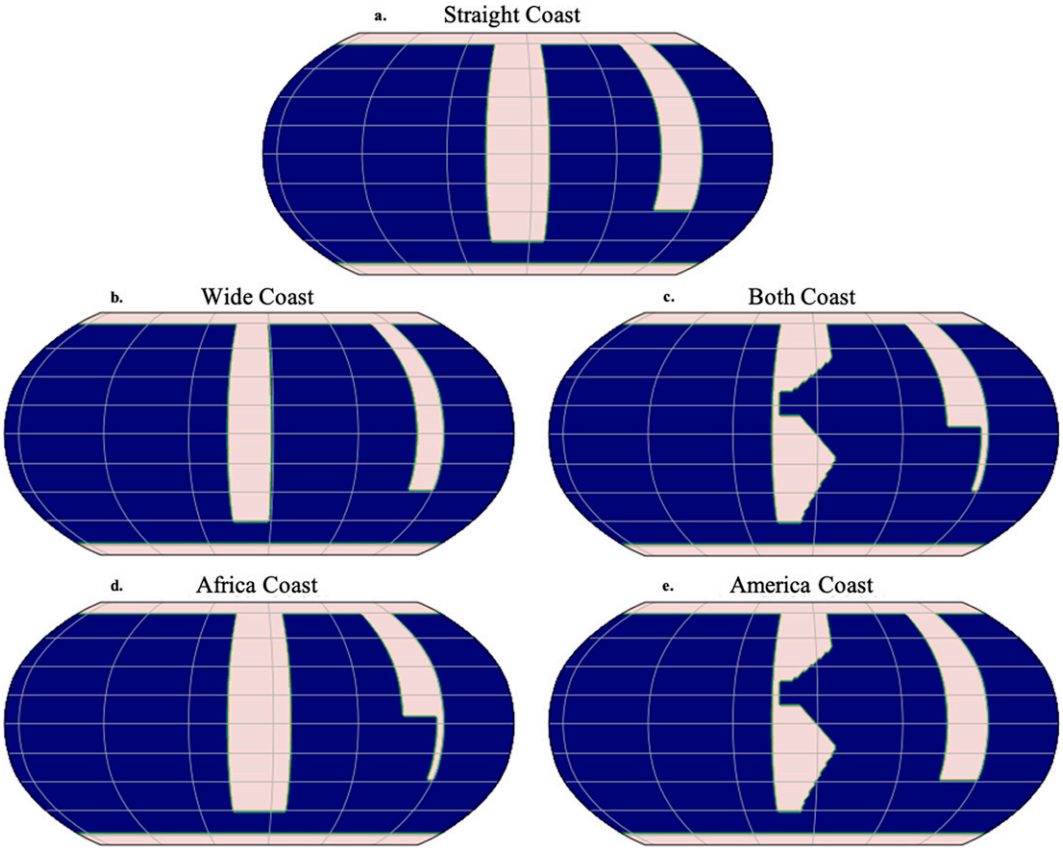

FIG. 1. Continental configurations for each of the simulations. Gray regions indicate land, and blue indicates ocean. The land boundaries are vertical, and the ocean is everywhere 5000 m deep and devoid of bathymetry.

these idealized configurations; rather the deepest mixed layers are in the northern Atlantic-like basin.

To balance the momentum input by the wind, a strong bottom drag is applied as a turbulent viscosity ν_{BBL} in the bottom boundary layer according to $\nu_{\mathrm{BBL}} = c_d|\mathbf{u}|\mathbf{u}$, where c_d is a nondimensional drag coefficient (we use a value of 0.03, a 10-fold increase over the standard value to account for the lack of bathymetry) and $\mathbf{u}$ is the velocity in the bottom boundary layer. Additional vertical turbulence parameterizations include the energetic planetary boundary layer scheme (Reichl and Hallberg 2018) and a small-scale, shear-driven mixing scheme (Jackson et al. 2008). A constant background diapycnal diffusivity of 2.0×10^{-5} m^2 s^{-1} is equal across simulations. Horizontal eddy effects are parameterized using a uniform background Laplacian horizontal viscosity of 20 000 m^2 s^{-1}, an eddy isopycnal thickness diffusivity coefficient (after Gent and McWilliams 1990) of 1000 m^2 s^{-1}, and an isoneutral diffusion diffusivity (Shao et al. 2020) of 1200 m^2 s^{-1}.

Unlike in previous idealized studies of the dependence of AMOC on basin geometry, here we include interactive sea ice using the GFDL Sea Ice Simulator, version 2 (SIS2) (Adcroft et al. 2019). SIS2 includes full ice dynamics with an elastic–viscous–plastic rheology and calculates the concentration, thickness, brine content, and snow cover of sea ice.

b. Atmospheric forcing

We run the ocean–sea ice model with atmospheric forcing that is derived from the Coordinated Ocean-Ice Reference Experiments (CORE) corrected normal year of forcing, version 2.0 (CNYF2), for ocean-ice simulations (Large and Yeager 2004). To guarantee that asymmetries between basins and differences between model simulations arise solely from ocean circulation and sea ice, we mask out land points in the CNYF2 dataset then perform a zonal average across all longitudes. To ensure that the forcing is hemispherically symmetric, we mirror the Southern Hemisphere data across the equator but maintain a seasonal cycle by lagging the Northern Hemisphere by 6 months. We apply this same procedure to all surface fields: shortwave radiation, longwave radiation, precipitation, 10-m meridional wind speed, and 10-m air temperature (all shown in Fig. 2). The surface forcings are calculated using bulk formulas (Fairall et al. 2003) from the modified atmosphere fields.

Sea level pressure is taken to be a constant, globally uniform value of 101 kPa. Wind speed is purely zonal in direction with meridional wind speeds set to zero everywhere. From the land caps to 50°N/S, the wind speed profiles are smoothed with a Savitsky–Golay filter using a fifth-order polynomial to allow wind speed to go smoothly to zero at the edge of the polar land caps.

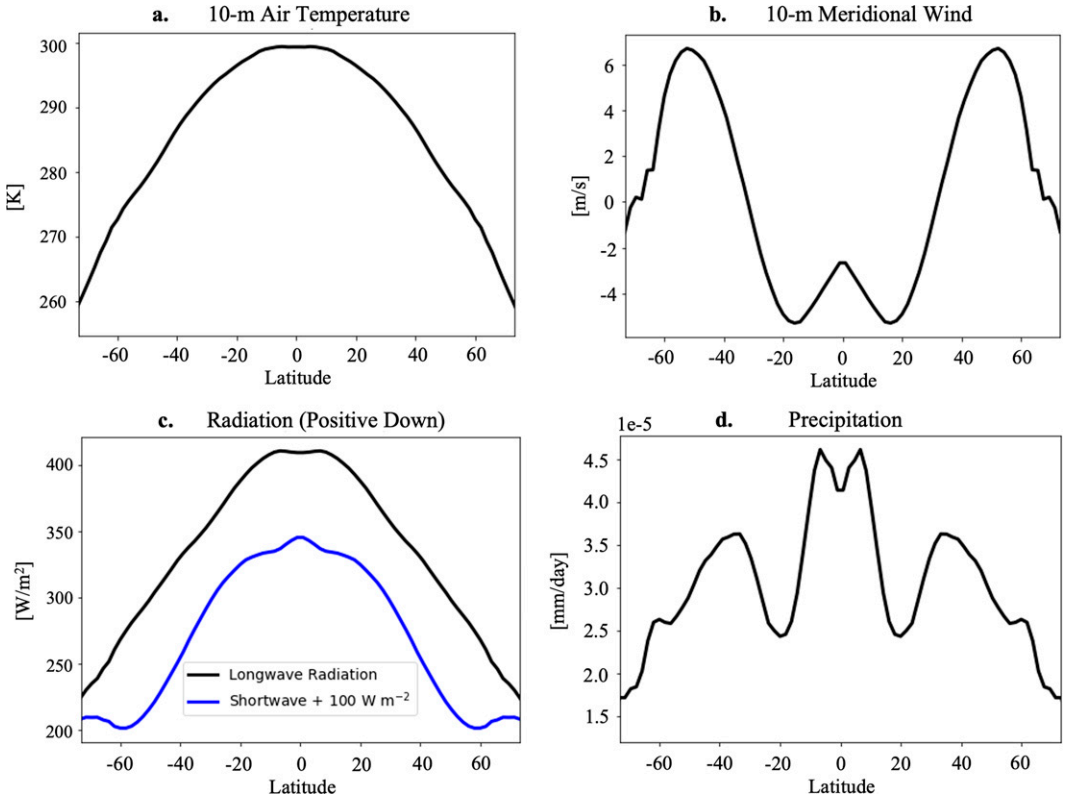

FIG. 2. Annual mean values of the modified CORE Normal Year Forcing 2.0 used to force the ocean–sea ice model: (a) 10-m air temperature, (b) 10-m meridional wind speed, (c) downwelling shortwave radiation and downwelling longwave radiation, and (d) precipitation.

Surface salinity flux adjustment is necessary to account for net nonzero freshwater flux at the surface arising from nonzero global precipitation minus evaporation ($P - E$). To maintain conservation of freshwater, $P - E$ is adjusted by scaling with a virtual precipitation at each coupling time step to ensure a globally integrated net zero freshwater flux while maintaining the correct pattern of global $P - E$.

The simulations (Fig. 1) start from rest and are integrated for one thousand 365-day years to equilibrium. Temperature and salinity are initiated from zonally averaged fields derived from a MOM6 aquaplanet simulation without continents. We perform all analyses on model climatologies produced by the last 100 years of the runs, and as such, we do not discuss variability in the runs. The only difference between each model simulation is the continental geometry along the Atlantic basin.

c. Continental configurations

Each of the five simulations has two meridional continents and two ocean basins: one wide, Pacific-like basin and one narrow, Atlantic-like basin (Fig. 1). In all cases, the western boundary of the Atlantic-like basin terminates at 55°S and the eastern boundary of the Atlantic-like basin terminates at 35°S. The simplest of our basin configurations, Straight Coast, features straight, meridional coastlines (Fig. 1a). Wide Coast widens the Atlantic-like basin while keeping the boundaries strictly meridional (Fig. 1b). Both Coast widens the Atlantic-like basin by the same average area as Wide Coast but does so by cutting out idealized shaped coastlines on both sides of the basin to resemble the east coast of the Americas and the west coast of Africa. Africa Coast has an Eastern boundary shape that is modified to resemble the African west coast to explore the effect of changing only the shape of the eastern boundary (Fig. 1d). America Coast has a western boundary shape that is modified to resemble the east coast of the Americas to explore the effect of changing only the shape of the western boundary (Fig. 1e). The average width and area of the Atlantic-like basin for each configuration is listed in Table 1.

3. Results

a. Response to changes in continental configuration

The Straight Coast is chosen as our reference-case experiment because its average Atlantic-like width and area are similar to the real Atlantic Ocean whereas the other configurations represent a widening of the Atlantic-like basin relative to Straight Coast. Straight Coast shows patterns of sea surface temperature (SST) and sea surface salinity (SSS) that are similar to what is observed in the world oceans: SST is highest in the tropics and decreases toward the poles; there is an

TABLE 1. List of model configuration names, average Atlantic-like basin width from the southern tip of the African continent, average Atlantic-like basin width between 20° and 60°N [L_x in Eq. (3)], Atlantic-like basin area, and Global ocean area.

Simulation	Mean Atlantic width (km)	Mean Atlantic width 20–60°N (L_x) (km)	Atlantic basin area (km^2)	Global ocean area (km^2)
Straight Coast	7200	6700	0.87×10^8	4.0×10^8
Both Coast	9400	8200	1.1×10^8	4.3×10^8
Wide Coast	9300	8700	1.1×10^8	4.3×10^8
America Coast	8500	8200	1.0×10^8	4.2×10^8
Africa Coast	8100	6700	0.98×10^8	4.1×10^8

equatorial cold tongue where water upwells to the surface; and SSTs in the northern high latitudes are greater in the small, Atlantic-like basin than in the large, Pacific-like basin by about 5°C (Fig. 3a). The salinity has maxima in the subtropical regions and minima in the tropics and subpolar to polar regions (Fig. 3b) and is elevated in the small Atlantic-like basin by about 3 practical salinity units (psu) relative to the large basin at 60°N. The North Atlantic–like basin is also less stratified than the North Pacific–like basin. The difference in density between 100 m and the surface, $\Delta\rho_z$ is smaller in the narrow basin than the large basin (Fig. 3c). While the precipitation is supplied as a boundary condition (Fig. 2d), the evaporation is allowed to evolve and follows a similar pattern to the SST. The evaporation minus the precipitation (Fig. 3d) highlights the subtropics as a region of excess evaporation while the subpolar regions and the equatorial cold tongues have more precipitation.

Consistent with previous studies (e.g., Ferreira et al. 2010; Nilsson et al. 2013; Cessi and Jones 2017; Jones and Cessi 2017), we find deep-water formation in the northern Atlantic-like basin (Fig. 4a) but not in the Pacific-like basin. A strong cross-equatorial meridional overturning circulation exists in the small, Atlantic-like basin, while a weaker, counterrotating deep cell penetrates into the large, Pacific-like basin (Fig. 4b). Sea ice is present year-round in the Southern Ocean and in the northern Pacific-like basin, while in the northern Atlantic-like basin a negligible amount of sea ice forms during the winter.

To compare sea surface properties across cases, we subtract the zonal mean of SST and SSS for Straight Coast from each configuration. The Both Coast Atlantic-like basin SST is warmer than Straight Coast by about 3°C (Fig. 5a) and the northern high-latitude SSS in the Atlantic-like basin is 2 psu greater than Straight Coast (Fig. 6a). For Wide Coast, the northern Atlantic-like basin SST is about 2°C warmer than for Straight Coast (Fig. 5b) and the basin SSS is about 2 psu greater (Fig. 6b). Cases with shaped western boundaries result in lower eastern equatorial SSS than do cases without.

The Both Coast, America Coast, and Africa Coast simulations all show similar SST and SSS anomalies (taken relative to Straight Coast). In the narrow basin, America Coast and Africa Coast have warmer SSTs than Straight Coast and show a pattern of zonal mean differences in SST from Straight Coast that is very similar to Both Coast (Figs. 5c,d). The

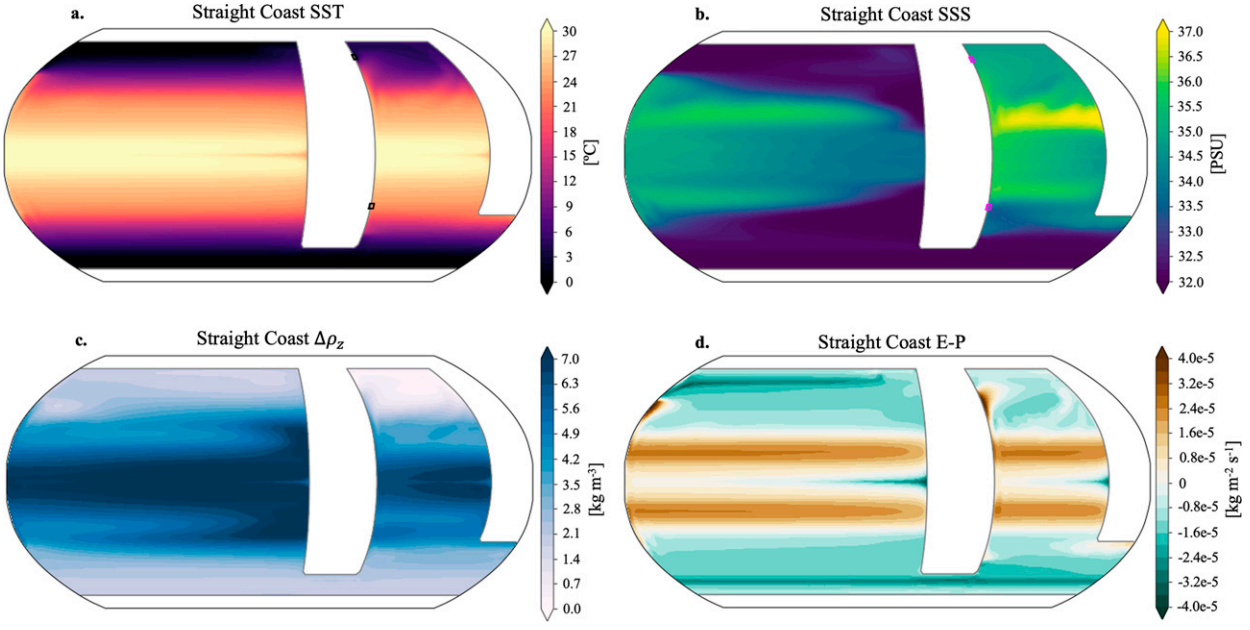

FIG. 3. Maps of (a) sea surface temperature, (b) sea surface salinity, (c) difference in density between 1000 m and the surface ($\Delta\rho_z$), and (d) evaporation minus precipitation for the Straight Coast continental configuration.

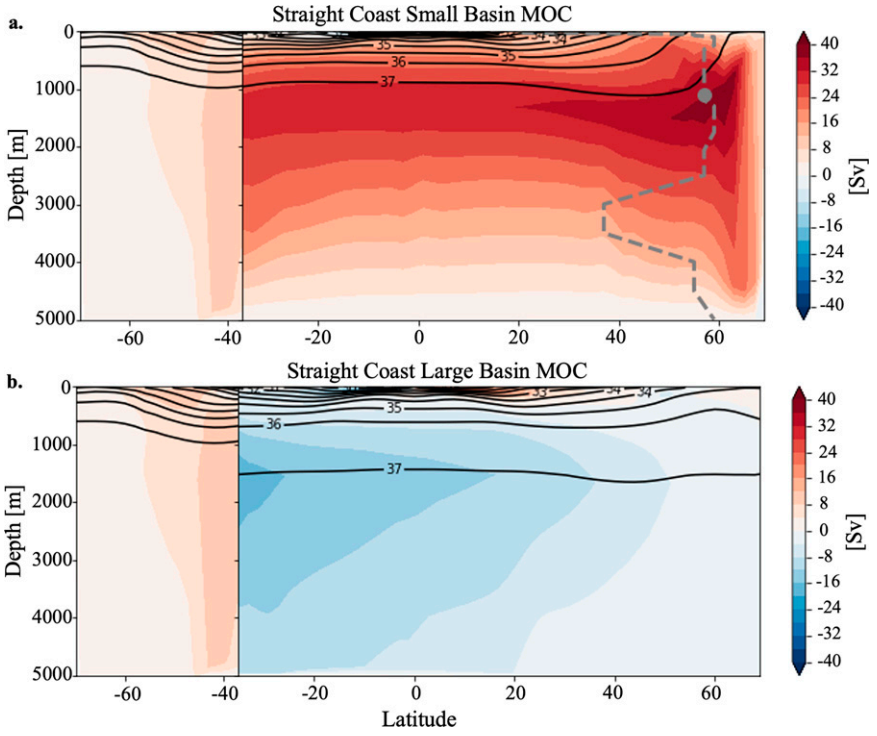

FIG. 4. Meridional overturning circulation for the Straight Coast case in (a) the small, Atlantic-like basin and (b) the large, Pacific-like basin. The southern ocean region in both plots shows the streamfunction integrated over all longitudes.

pattern of SSS changes in America Coast is similar to the changes in Both Coast, with decreases in the eastern tropics and increases in the northern subpolar region (Fig. 6c). The SSS in Africa Coast shows a similar pattern to America Coast, but with a smaller decrease in SSS in the eastern tropics than America Coast and Both Coast (Fig. 6d). These changes in SST and SSS result in a small density increase in the northern high latitudes in the narrow basin.

The changes between configurations can be seen deeper in the water column as well. Changes in the zonal mean density difference between 1000 m and the surface ($\Delta\rho_z$), relative to what is seen in Straight Coast reveal differences in stratification between configurations (Fig. 7). The stratification in Straight Coast is weakest in the northern part of the basin, near 60°N (Fig. 7a). In all of the other configurations (Figs. 7b–e), the stratification decreases over the majority of the Atlantic-like basin, with the largest differences in the subpolar regions just south of 60°N. In general, each of the other cases is warmer, saltier, and more weakly stratified than Straight Coast, making the northern Atlantic-like basin more favorable for deep ventilation.

In each of the configurations, deep ventilation and cross-equatorial model meridional overturning circulation (MOC) are confined to the Atlantic-like basin. Deep water formed at the northern edge of the basin flows southward at depth. It upwells in the Southern Ocean and is replenished by northward flowing shallow water (Fig. 4). MOC is calculated on isopycnal surfaces and remapped to depth space for plotting purposes. As in previous studies, the MOC is localized to the narrower basin with a eastern boundary that terminates north of the zero wind stress line in the Southern Hemisphere (Ferreira et al. 2010; Nilsson et al. 2003; Cessi and Jones 2017; Jones and Cessi 2017; Youngs et al. 2020). This can be attributed to the higher salinity of the narrow basin driven by greater evaporation over the warmer SSTs in our simulations. In turn, the warmer SSTs in the narrow basin are due to changes in ocean circulation from changing the geometry of the ocean basin.

While surface conditions look similar across each configuration, small changes in stratification in the northern Atlantic-like basin (Fig. 7) are enough to drive significant changes in the meridional overturning circulation (Fig. 8). In Both Coast, the overturning in the Atlantic-like basin shoals relative to Straight Coast (Fig. 8a) with MOC increasing near the surface and decreasing at depth. At 1000 m and 60°N, Both Coast MOC is larger by about 6 Sv (1 Sv $\equiv 10^6$ m^3 s^{-1}). In addition, the MOC in Both Coast (which has more realistic coastlines than Straight Coast) more closely represents the canonical AMOC—the model MOC shoals to allow for a deep, counterclockwise overturning cell. The increase in MOC for both Wide Coast and Both Coast differs from Jones and Cessi (2017) who found an increase in basin width resulted in an overall decrease in AMOC strength (see section 4). MOC in Wide Coast is larger than in Straight Coast, particularly below 1500 m, with the exception of a small region of weaker circulation at the northern edge of the basin near the surface (Fig. 8b). At 1000 m and 60°N, the depth and latitude of

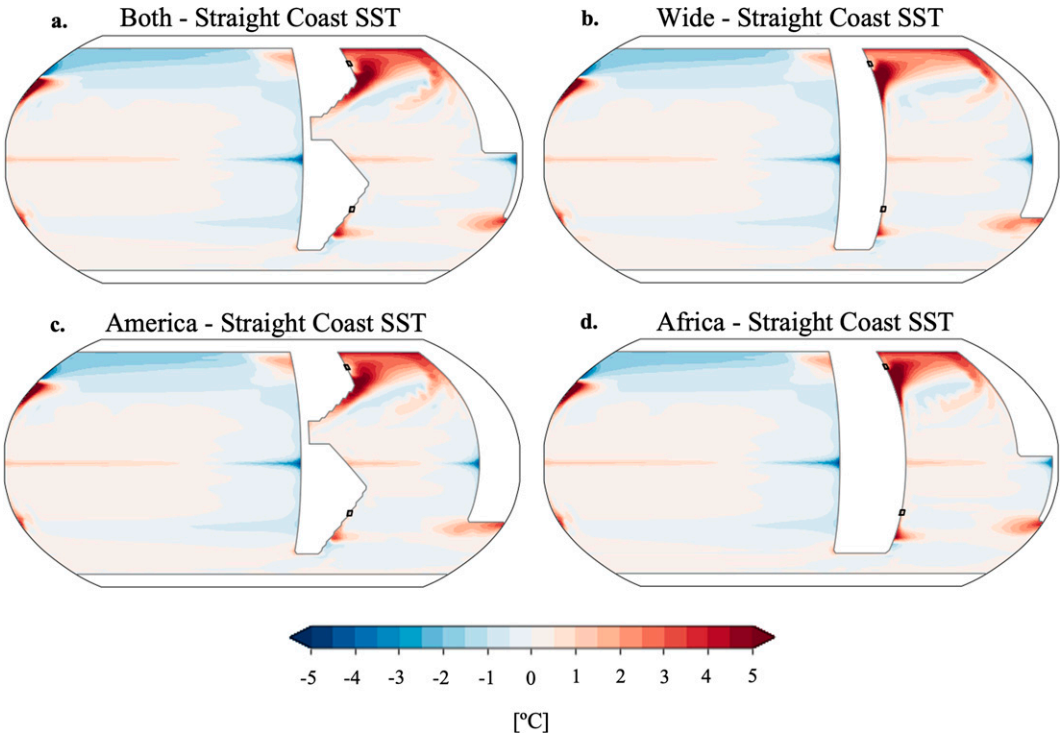

FIG. 5. Climatological sea surface temperature anomalies from Straight Coast global zonal mean SST for (a) Both Coast, (b) Wide Coast, (c) America Coast, and (d) Africa Coast.

maximum MOC, the Wide Coast MOC is larger than Straight Coast MOC by 10 Sv (Table 2; Fig. 9).

Changing the shape of the western boundary, as represented by America Coast, results in an increased MOC strength and a MOC deepening (Fig. 8c). However, changing the eastern boundary, as in Africa Coast, results in a shoaling of the MOC (Fig. 8d) and larger changes in the abyssal ocean circulation than in the upper ocean. The changes in MOC in Both Coast reflect the impact of a shaped western boundary and a shaped eastern boundary. The simple linear summation of the magnitudes of the maximum MOC anomaly (relative to Straight Coast) from Africa Coast and America Coast is similar to that of Both Coast—6.6 Sv versus 6.3 Sv, respectively. This linearity also holds for the vertical and meridional structure of MOC, which allows us to attribute anomalies in the Both Coast simulation to either one coastline or the other. Changing the western boundary shape results in much larger differences in MOC strength than changing the eastern boundary shape.

As the overturning circulation in the small, Atlantic-like basin responds to changes in coastline shape, the overturning in the abyssal large, Indo-Pacific-like basin acts to compensate those changes, such that as AMOC increases, the deep Indo-Pacific overturning decreases (Sun et al. 2020). Here, in response to a strengthening of MOC in the Atlantic-like basin, the deep overturning streamfunction associated with upwelling in the large, Indo-Pacific-like basin intensifies, bringing more deep water northward and more intermediate water southward (Figs. 8e–h).

Widening the Atlantic-like basin with straight coastlines (Wide Coast), results in a different change in MOC than widening the Atlantic-like basin by changing the shape of the coastlines (Both Coast), despite equal basin-average widths over the length of the basin (between 35°S and 70°N). Thus, changes in MOC strength cannot be predicted based on changes in average basin width alone—the shape of the basin boundaries also matters. Differences in coastline shape along the Atlantic-like basin lead to distinct sea surface properties and meridional overturnings in each experiment. Moreover, widening the Atlantic by changing the shape of the eastern boundary of the basin results in distinct impacts on sea surface properties, MOC, and abyssal circulation as compared with widening the Atlantic by changing the shape of the western boundary. Indeed, the shape of the basin, or more specifically the shape of the western and eastern coastlines along the basin, is just as important if not more important than the width of the basin, even when taking into account the change in width with latitude. We performed an additional simulation in which we mirrored the realistic American coastline onto the African continent (while leaving a straight western boundary); this configuration (not shown) produces a vastly different AMOC than the America Coast configuration, consistent with our above findings that the shape of the coastlines—rather than simply the basin width—influences the structure and strength of AMOC.

Deep ventilation and associated MOC are localized to the narrow basin because of its elevated salinity relative to the wide basin. At equilibrium, the transport of freshwater into an ocean

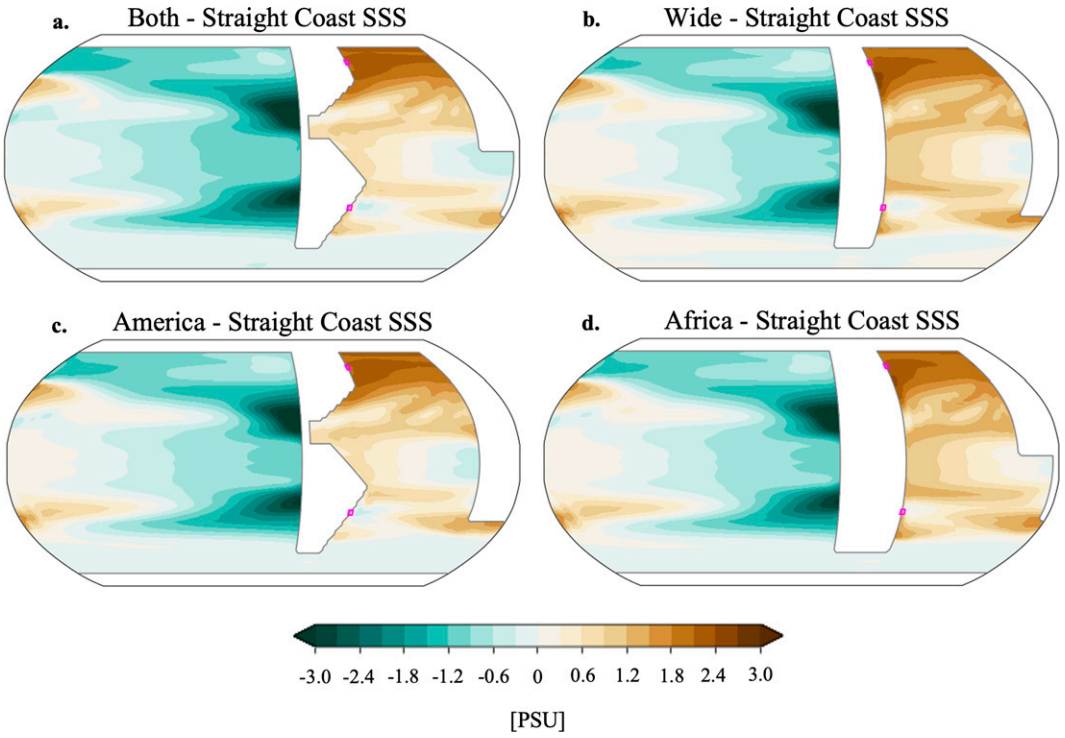

FIG. 6. Climatological sea surface salinity anomalies from zonal mean Straight Coast SSS for (a) Both Coast, (b) Wide Coast, (c) America Coast, and (d) Africa Coast.

basin must balance the total integrated surface freshwater flux over the basin. Thus, to examine the drivers of salinity differences between runs with different continental configurations, we calculate the freshwater transport into the Atlantic-like basin by integrating the surface freshwater terms:

$$F = \int_{y_S}^{y_N} \int_{x_W}^{x_E} (E - P)\, dx\, dy,$$

where $E - P$ is the net surface freshwater balance including evaporation, precipitation, runoff, and ice melt in units of meters per second. The integral extends from the western (x_W) to the eastern (x_E) boundaries of the Atlantic-like basin and from the southern boundary of the basin (y_S = 30°S) to the northern (y_N) continental boundary, because it is the freshwater transport at the southern boundary of the basin that is most relevant for the stability of MOC (Rahmstorf 1996).

Values for the Atlantic-like basin freshwater transport at 30°S are listed in Table 2. While configurations with narrower mean Atlantic widths and smaller Atlantic areas generally have greater values for freshwater transport, there are exceptions. For instance, Wide Coast has a wider basin than Both Coast and America Coast but has a smaller freshwater transport. A larger freshwater transport into the Atlantic-like basin is generally correlated with larger values of maximum AMOC across configurations. This arises because a larger AMOC corresponds to higher SSTs in the basin, which in turn corresponds to higher evaporation rates requiring larger freshwater transport to balance at equilibrium. Note that this is different from the simulations of Jones and Cessi (2017), who prescribe a zonally uniform net freshwater flux at the surface that cannot change with basin geometry, thus requiring no net change in freshwater input into the Atlantic-like basin to balance.

To summarize, the structure and strength of the MOC depend on the details of the Atlantic-like basin geometry, rather than simply the average width of that basin. A larger MOC corresponds to higher SST in the Atlantic-like basin that, via enhanced evaporation, causes higher salinity in that basin and thus greater surface density at high latitudes. The causal role of ocean transport of freshwater in MOC changes is complex, however, since the ocean actually transports more freshwater into the Atlantic-like basin when MOC is stronger and the basin is saltier (as is required to balance the salinity budget at equilibrium in these simulations). Any analysis to compare the relative roles of ocean circulation and surface freshwater forcing in setting the Atlantic-like basin's salinity would be purely diagnostic. In the next section, we instead attempt to better understand MOC changes by evaluating their relationship to the changes in basin-scale meridional density gradients that have resulted from the changes in coastline shape.

b. AMOC density scaling

The similar surface conditions across continental configurations (Figs. 5–7) belie the large differences in MOC strength and structure that occur when coastline shape is changed (Fig. 3). To investigate the relationship between basin geometry and

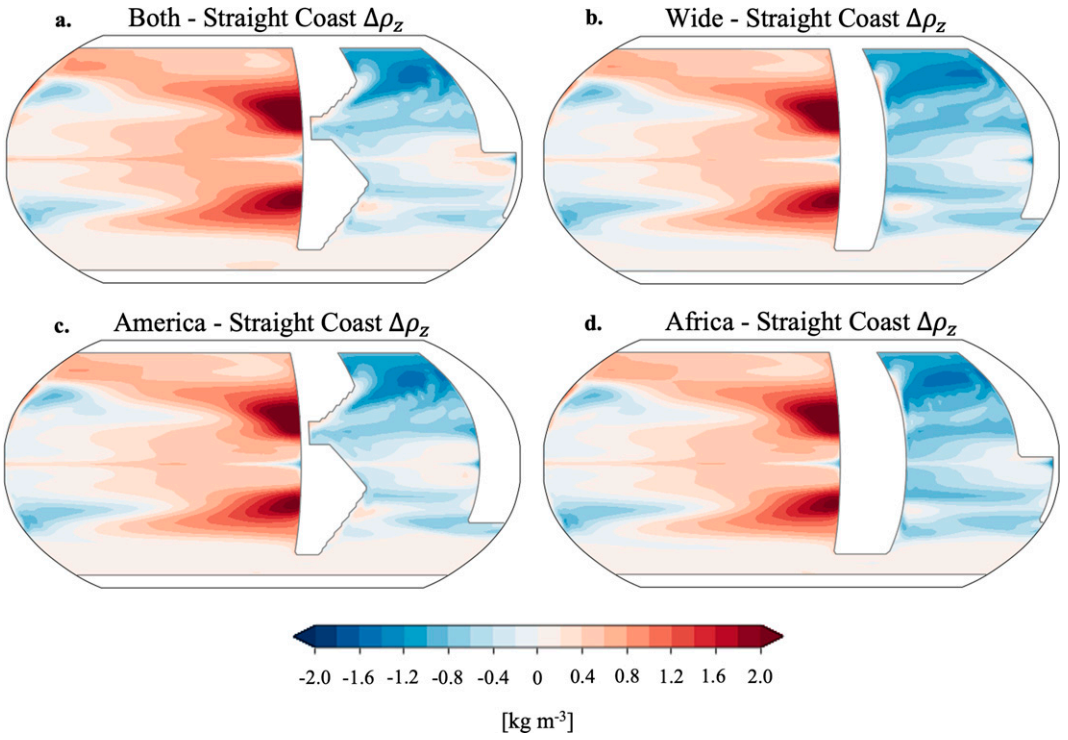

FIG. 7. Climatological $\Delta\rho_z$ (differences in density between 1000 m and the surface) anomalies from zonal mean Straight Coast $\Delta\rho_z$ for (a) Both Coast, (b) Wide Coast, (c) America Coast, and (d) Africa Coast.

meridional overturning circulation, we employ previously developed theory that relates AMOC to the basin-scale meridional density gradient. Theoretical approaches for understanding controls on overturning strength have been framed in terms of density gradient-driven gravity currents and have sought to relate the strength of meridional overturning in the Atlantic to the meridional density gradient (Thorpe et al. 2001; Delworth and Dixon 2006; Straneo 2006). Previous studies derived similar density scalings for AMOC (Robinson and Stommel 1959; Bryan 1987; Marotzke 1997; Gnanadesikan 1999; Thorpe et al. 2001; Griesel and Maqueda 2006). De Boer et al. (2010) explore several different variations of the relationship between MOC strength (denoted by Ψ) and the meridional density gradient (denoted by $\Delta\rho_y$): $\Psi \propto \Delta\rho_y H^2$, where H is a vertical scale depth. The most appropriate scale depth [as determined by De Boer et al. (2010)] is that derived from the meridional density gradient in the western boundary, where H is taken to be the depth at which the depth-integrated meridional density gradient equals the vertical mean of the depth-integrated meridional density gradient. This scale depth is linked to isopycnal slopes near the northern boundary of the basin and the available potential energy in the region, as well as to processes in the Southern Ocean (Gnanadesikan 1999; Wolfe and Cessi 2010; Sijp et al. 2012). We adopt this interpretation here while retaining a depth dependence, following a method described by Butler et al. (2016).

We apply theory developed by Butler et al. (2016) as a framework for comparing the results of the different simulations. Butler et al. (2016) makes the following assumptions: 1) the large-scale ocean circulation is geostrophic; 2) thermal wind balance holds over the entire area and depth range of interest; and 3) the meridional density gradient is proportional to the zonal density gradient, such that

$$\frac{\Delta\rho_x(z)}{L_x} = c\frac{\Delta\rho_y(z)}{L_y},$$

where c is some dimensionless constant of proportionality, $\Delta\rho_x$ is the zonal density gradient, L_x is the zonal width of the basin between 20° and 60°N, $\Delta\rho_y$ is the meridional density gradient, and L_y is the meridional length. Zonal and meridional pressure and density gradients are closely related provided that the large-scale circulation is geostrophic. This relationship is found to hold at equilibrium in an idealized modeling study (Park and Bryan 2000). Moreover, meridional pressure gradients drive zonal eastward flows, which converge at the eastern boundary of the ocean basin, propping up a zonal pressure gradient. This zonal gradient in turn, sets up a meridional flow (Marotzke 1997; Kuhlbrodt et al. 2007). Another theory justifying the proportionality between zonal and meridional density gradients involves the propagation of fast boundary waves southward along the western boundary and across the equator to the eastern boundary; these waves are produced by a meridional density gradient along the western boundary of the basin (Johnson and Marshall 2002; Bell 2015; Johnson et al. 2019, and references therein).

By relating the zonal and meridional density gradient, the thermal wind relation can be scaled and rewritten to relate typical values for meridional velocity V to the meridional density difference $\Delta\rho_y$ (Butler et al. 2016):

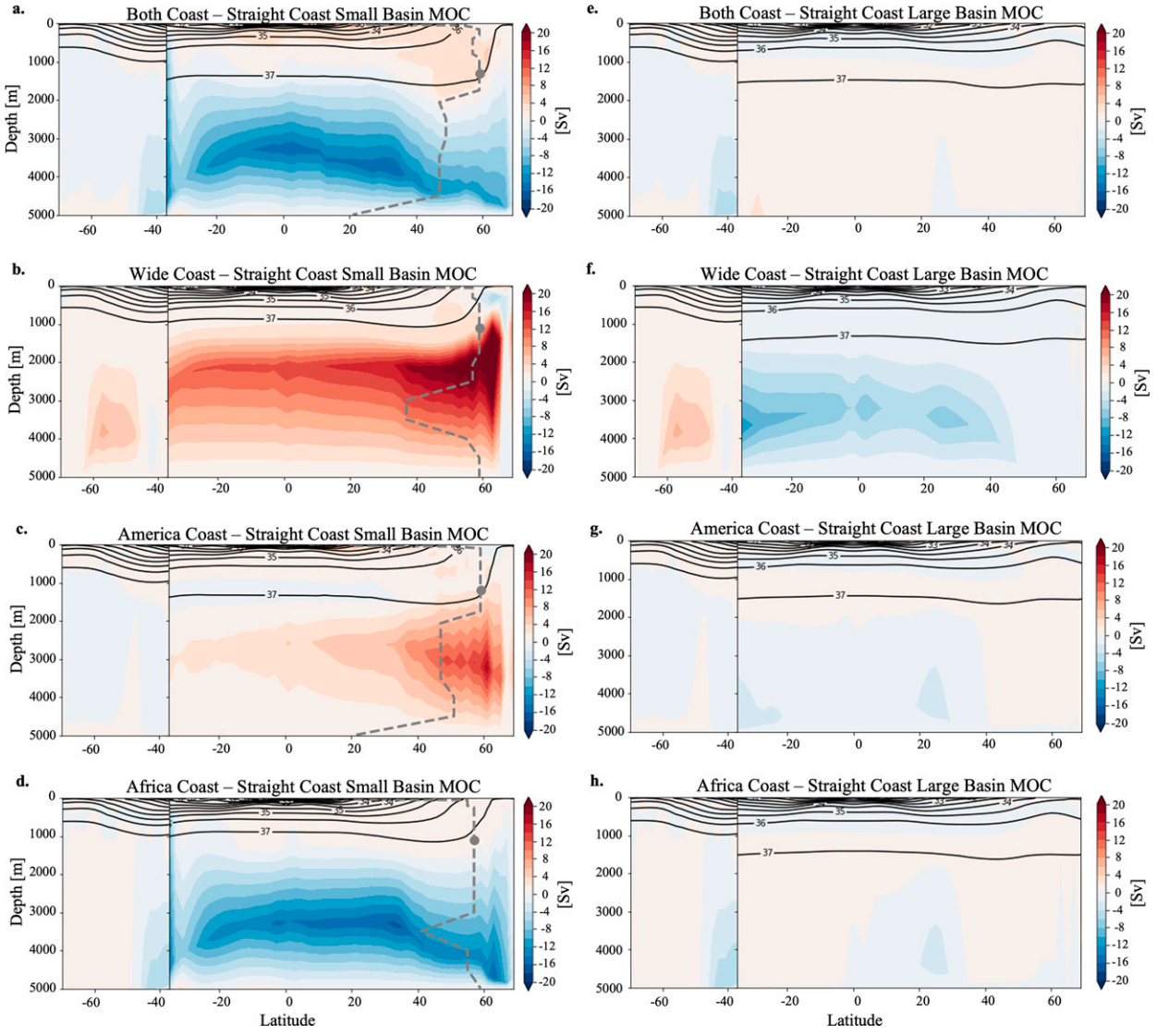

FIG. 8. Meridional overturning circulation anomaly from Straight Coast in the (left) Atlantic-like basin and (right) Pacific-like basin for (a),(e) Both Coast; (b),(f) Wide Coast; (c),(g) America Coast; and (d),(h) Africa Coast. The gray dashed line indicates the latitude of the maximum MOC at each depth plotted in Fig. 9, below, and the gray circle indicates the depth and latitude of the maximum MOC. Black contours indicate density surfaces.

$$\frac{\partial V}{\partial z} = \frac{cg}{f_0 \rho_0} \frac{\Delta \rho_y(z)}{L_y}, \tag{1}$$

where g is the gravitational acceleration, f_0 is a typical value for the Coriolis parameter, and ρ_0 is the reference density. Equation (1) can then be integrated with respect to depth to find an expression for the characteristic meridional velocity and still retain the depth dependence of the meridional density difference (Butler et al. 2016):

$$V(z) = \frac{cg}{f_0 \rho_0 L_y} \left\{ \frac{1}{D} \int_{-D}^{0} \left[\int_{z'}^{0} \Delta \rho_y(z'')\, dz'' \right] dz' - \int_{z}^{0} \Delta \rho_y(z')\, dz' \right\} \tag{2}$$

where D is the ocean depth. The constant of integration is constrained by the fact that there is no net meridional flow and, as such, cannot be zero. Butler et al. (2016) show that the constant of integration is

$$\frac{cg}{f_0 \rho_0 L_y} \left\{ \frac{1}{D} \int_{-D}^{0} \left[\int_{z'}^{0} \Delta \rho_y(z'')\, dz'' \right] dz' \right\}.$$

Integrating Eq. (2) and assuming vertical side walls results in an expression for the meridional overturning circulation Ψ:

$$\Psi(z) = L_x \int_{z}^{0} V(z)\, dz. \tag{3}$$

TABLE 2. List of model output maximum MOC values and associated depths for each simulation, along with maximum MOC and depth predicted from the meridional density difference scaling. Also included are the maximum barotropic streamfunction values for the northern subtropical and subpolar gyres in the Atlantic-like basin. The final column lists values of the inferred freshwater transport F at 30°S in the Atlantic-like basin, calculated by integrating the surface freshwater balance as described in section 3a.

Simulation	Max MOC (Sv)	Max MOC depth (m)	Predicted MOC (Sv)	Predicted MOC depth (m)	Subtropical barotropic streamfunction (Sv)	Subpolar barotropic streamfunction (Sv)	Atlantic freshwater transport F (Sv)
Straight Coast	28.3	1100	25.6	1000	22.1	21.5	0.44
Both Coast	34.6	1300	38.6	1000	24.2	21.8	0.64
Wide Coast	38.5	1100	41.1	1200	31.5	26.6	0.54
America Coast	34.4	1200	37.4	1100	23.9	21.9	0.56
Africa Coast	28.8	1100	27.6	900	22.1	21.0	0.53

As defined in Eq. (3), there is a positive relationship between the magnitude of the twice-integrated density difference between northern and southern points in the Atlantic-like basin $\left(\int\int \Delta\rho_y\, dz\, dz\right)$ and MOC. As the meridional density difference increases, so too does the meridional overturning. The derivation of Eq. (3) assumes straight meridional boundaries along the basin and excludes any consideration of coastline shape. Applying the scaling to the configurations in this study tests how well the relationship between MOC and meridional density gradient holds when the assumption of straight coastlines is relaxed and gives insight into how the meridional density structure is linked to MOC.

Unlike other AMOC scalings that rely on the density at specific depths, the Butler et al. (2016) relationship [Eq. (3)] uses the entire vertical structure of density and results in an estimate of MOC as a function of depth. Here, we interpret this as the structure of the maximum MOC at each depth within the Atlantic basin. The density structure can be influenced by both changes in ocean circulation and surface freshwater forcing, both of which are driven by changes in basin geometry.

We use the scaling described in Eq. (3) to calculate the MOC in the narrow basin of each simulation. Maximum MOC predicted from the Butler et al. (2016) scaling (hereinafter Ψ_B) for each case are shown in Fig. 9. Here, the meridional density difference, $\Delta\rho_y$ is taken as the difference in density between 60°N and 30°S one grid point away from the western boundary of the Atlantic-like basin. The locations from which the density differences are calculated are indicated with gray and pink boxes in Figs. 3, 5, and 6. The basin width L_x is taken as the average basin width between 20° and 60°N for each configuration. Values for L_x are listed in Table 1. The constant of proportionality, $c = 0.96$, that is used to calculate Ψ_B is the same value across all of the simulations and is the value reported in Butler et al. (2016).

While the values of the maximum model MOC (hereinafter $\Psi_{\max}$) and Ψ_B differ somewhat, the ranking of $\Psi_{\max}$ and Ψ_B from weakest to strongest agree well (Table 2). This suggests that Eq. (3) can provide insight into how MOC depends on basin shape. Further examination of the relative vertical structures of $\Psi_{\max}$ and Ψ_B shows qualitative agreement as well (Fig. 9): $\Psi_{\max}$ and Ψ_B for Straight Coast and Africa Coast are similar to each other, as are $\Psi_{\max}$ and Ψ_B for America Coast and Both Coast. This suggests that the shape of the North American coast is particularly important in the vertical structure of MOC via changes in meridional density gradient along the western boundary of the basin, while the shape of the African coast plays a smaller role.

What causes changes in meridional density gradients, and thus Ψ_B, between the different continental configurations? Changes in the twice-integrated density at either the northern or southern end of the Atlantic-like basin are similar to each other across continental configurations, and much larger than the changes across configurations in twice-integrated density differences themselves (Figs. 10a,b). Thus, changes in meridional density gradients cannot be explained by changes at surface in the northern end of the Atlantic-like basin.

Moreover, changes in meridional density gradients cannot be described by changes in temperature or salinity alone. We calculate $\int\int \Delta\rho_y\, dz\, dz$ using a fixed-temperature meridional density gradient and a fixed-salinity meridional density gradient but find little correlation between the double-integral and MOC strength. Changes in both temperature and salinity contribute to the changes in density between the experiments in complex ways.

Sensitivity tests reveal that the MOC scaling [Eq. (3)] is relatively unaffected by changes in latitude for both the northern and southern regions used to calculate the meridional density difference (not shown). Moreover, the basin width L_x that produces the best fit to the model output MOC is the average width between 20° and 60°N rather than the average width of the entire basin. While the Butler model assumes straight boundaries, it can in fact predict overturning in basins with shaped sidewalls, provided the choice of L_x describes the width of the northern basin. This indicates that shape, and not only basin width, matters for the meridional density gradient and thus the overturning strength.

4. Discussion and conclusions

Previous studies have shown that the relatively narrow basin width and the southern extent of the continents provide

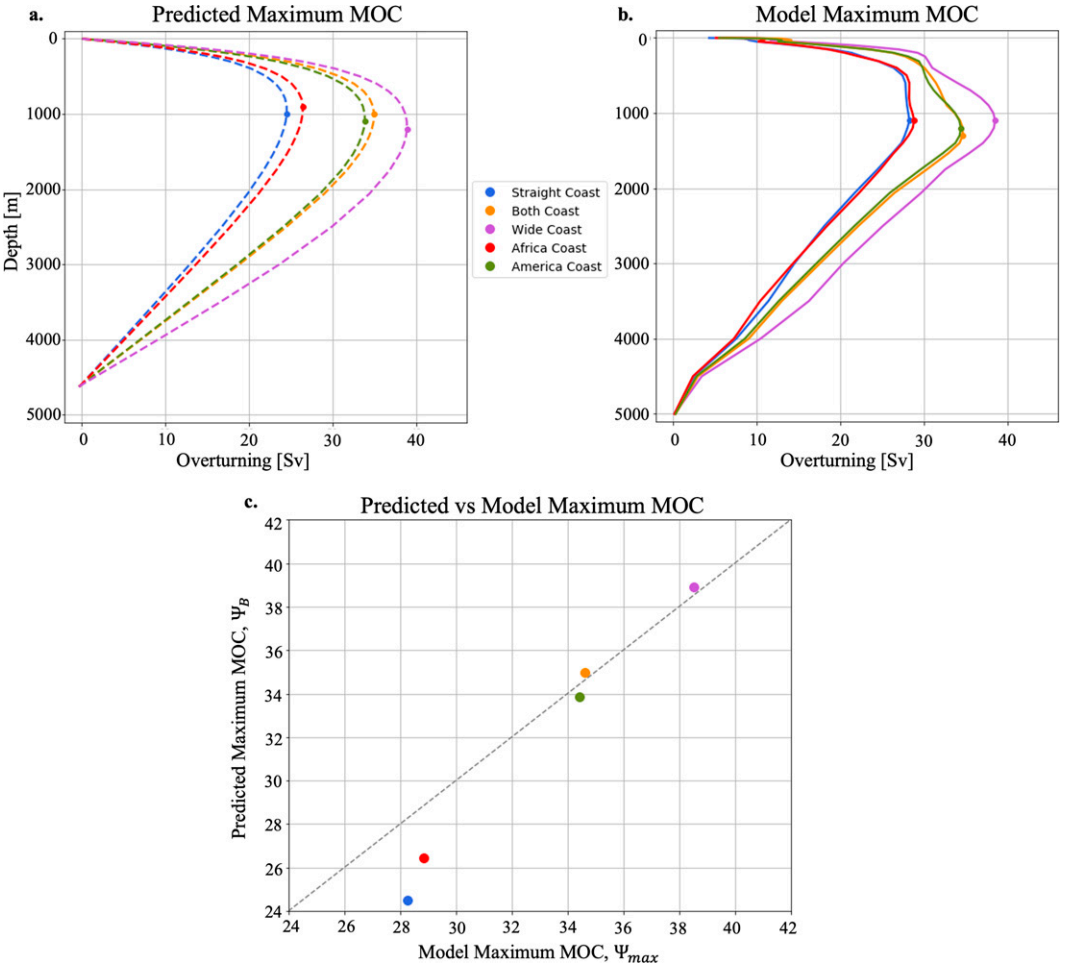

FIG. 9. (a) Maximum MOC $\Psi_{\max}$ calculated from the model at each depth level between 30°S and 50°N for each case, (b) maximum MOC Ψ_B predicted by the Butler scaling Eq. (3) strength at each depth calculated by twice integrating the meridional density difference, and (c) Ψ_B plotted against $\Psi_{\max}$.

important geometric constraints on the localization of deep-water formation in the Atlantic Ocean (Ferreira et al. 2010; Nilsson et al. 2013; Jones and Cessi 2017; Cessi and Jones 2017; Youngs et al. 2020). Here we examine the impacts of coastline geometry on meridional overturning circulation in a narrow, Atlantic-like basin in five ocean-only idealized continental configurations that range from coastlines that are straight to coastlines shaped like the American and African continents.

A primary finding is that overturning circulation changes that occur when widening the Atlantic basin by changing the coastline shape (Both Coast) are distinct from those that arise when widening the Atlantic basin without modifying the coastline shape (Wide Coast), even when the average basin widths and areas increase by the same amount (Table 1). While generally we see an increase in MOC strength with basin width, this relationship is not linear; configurations with the same western boundary shape have similar MOC strengths despite differences in mean basin width (with the exception of Wide Coast, which has a stronger MOC than all other cases).

Note that because our atmospheric forcing is zonally symmetric and constant across configurations, any asymmetries that arise between basins or between configurations must be due to differences in ocean circulation driven by changes in the coastline geometry of the Atlantic basin. Freshwater forcing at the ocean surface can drive differences between configurations, but the evaporation responds to SST changes that are due to circulation changes (while precipitation is zonally uniform and constant across configurations). While the basin width and shape as well as the basin evaporation minus precipitation both impact the oceanic freshwater transport, the changes all arise due to the change in coastline geometry between simulations. The freshwater transport at the south of the Atlantic-like basin is controlled both by basin size and by the surface freshwater balance and is not perfectly correlated with the MOC strength. Moreover, the freshwater balance at the surface is influenced by the SSTs, which are influenced by

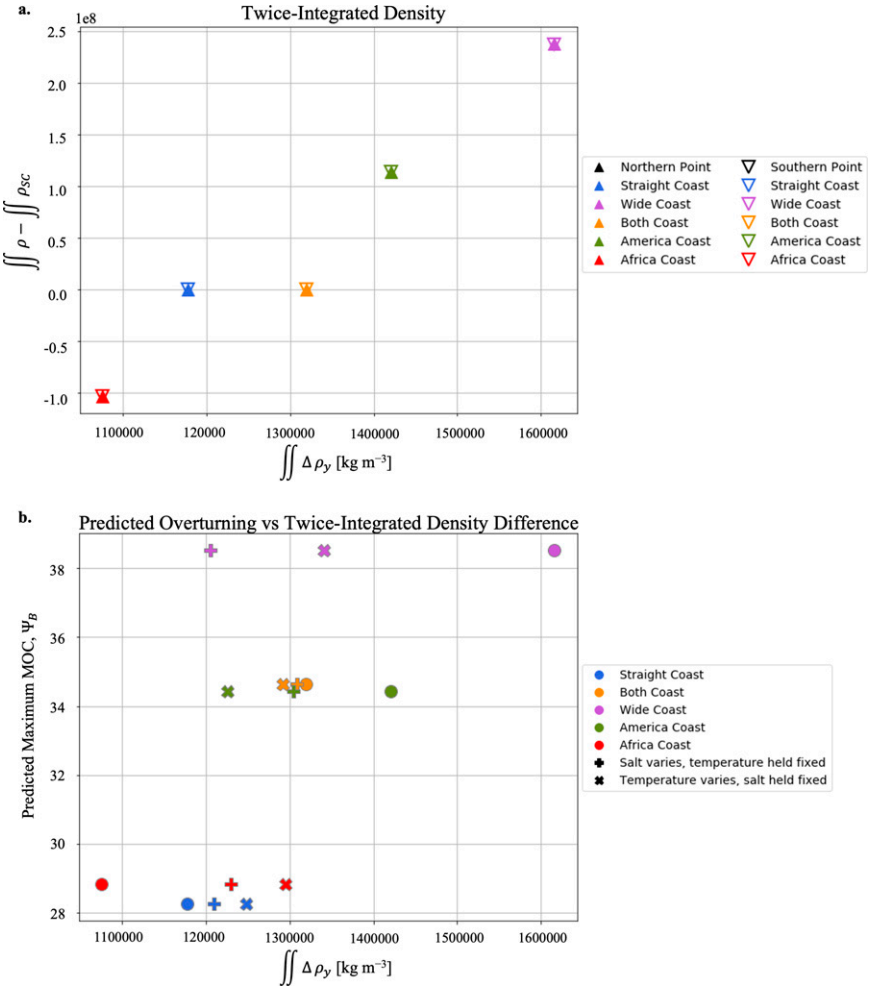

FIG. 10. (a) Twice-integrated density anomaly from Straight Coast, $\iint \rho - \iint \rho_{sc}$, at both the northern and southern ends of the domain is plotted against the twice-integrated meridional density difference $\iint \rho_y$. (b) Predicted overturning plotted against twice-integrated meridional density difference, plotted with circles. Also shown is predicted overturning plotted against twice-integrated meridional density difference calculated with fixed temperature Θ_0 or fixed salinity S_0. Density differences calculated with fixed temperature are indicated with a plus sign, and density differences calculated with fixed salinity are indicated with a times sign.

ocean circulation changes that arise from changing the shape of the coastline.

Each of the Wide Coast, Both Coast, America Coast, and Africa Coast cases represents a widening of the Atlantic-like basin with respect to the Straight Coast control case. Widening the basin results in warmer northern Atlantic-like basin SSTs (Fig. 5). Moreover, simulations with shaped western boundaries (Both Coast and America Coast) and those that do not (Wide Coast and Africa Coast) show different patterns of SST anomalies. Widening the Atlantic-like basin also results in higher basin-average SSS (Fig. 6). Stratification in the subpolar region of the Atlantic-like basin decreases in strength when the western boundary along the basin is shaped, rather than purely meridional (Fig. 7).

Both the western coastline and the eastern coastline play important roles in modulating the overturning circulation (Fig. 8). The simulations with shaped western coastlines (America Coast and Both Coast) show increased shallow overturning streamfunctions above approximately 1500 m relative to Straight Coast. This demonstrates that the shape of the American coast along the Atlantic basin is important for MOC vertical structure and strength. Simulations with shaped eastern coastlines (Both Coast and Africa Coast) show decreased abyssal overturning streamfunction and shoaled MOC relative to Straight Coast. Changes in abyssal circulation seen in Africa Coast highlight an apparent link between Atlantic abyssal circulation and the width of the Agulhas region. The shape of the African coast along the Atlantic is

important for the abyssal Atlantic circulation and the vertical structure of MOC but not for MOC strength.

In general, our results confirm the findings of previous studies that find that northern deep ventilation and associated cross-equatorial overturning circulation is confined to the narrower of two ocean basins. In our simulations, we see an increase in MOC strength with an increase in basin width. This is inconsistent with the results of Jones and Cessi (2017), who found that widening the Atlantic-like basin leads to a small decrease in MOC strength. This could, in part, be explained by differences in experimental design: the Jones and Cessi (2017) continental boundaries are thin, meridional ridges whereas ours are wider strips of land, some of which have more complex coastline shapes and could impact the relative contributions of "Warm Route" and "Cold Route" transport into the basin; their model does not include sea ice while ours does; they prescribe $P - E$ through a surface freshwater flux whereas our model allows evaporation to evolve with changing SST; and the surface forcings they use are constant in time and include a SST relaxation, which could constrain the SST more strongly. The simulations presented here include seasonality and use surface forcings calculated with bulk formulas from atmospheric products (CNYF2). Moreover, Jones and Cessi (2017) use a linear equation of state while MOM6 uses the nonlinear Wright equation of state (Wright 1997), which makes temperature less important for density at low temperature relative to a linear equation. One final difference is that in Jones and Cessi (2017), the total global ocean area remains constant while here, the different coastline configurations do have different global ocean areas (Table 1), providing a greater area over which water can upwell and that can allow for a larger MOC (Jones and Cessi 2016). Interestingly, AMOC strength (Table 2) does not scale linearly with narrow basin width, narrow basin area, total global ocean area, or freshwater transport into the narrow basin (Table 1), allowing for the possibility of the existence of the salt–advection feedback (Stommel 1961).

Jones and Cessi (2017) argue that an increase in basin width results in a greater Sverdrup gyre transport (Sverdrup 1947), and thus a stronger subpolar western boundary current. This acts to oppose the northward MOC component of the western boundary velocities. The MOC-associated subtropical transport can be modulated by nonlocal effects (Gnanadesikan 1999; Jones and Cessi 2017), and thus does not strengthen with increased basin width as the wind-driven subpolar western boundary current does. As such, in a narrower Atlantic basin, the subtropical western boundary current can flow farther north, bringing salty water with it. As this salty water flows north and cools, it increases in density, decreasing stratification and increases MOC. Other studies suggest that a wider basin could result in a larger magnitude in MOC due to a larger effective meridional diffusivity in wider basins (Wang et al. 1995; Nilsson et al. 2021). In a wider basin, the gyre and mesoscale eddy driven transport of salinity from the subtropical to subpolar gyre is greater, increasing northern salinity and density, thus creating favorable conditions for deep sinking. This transport also brings heat into the northern high latitudes, allowing for more evaporation, further increasing the northern high-latitude salinity.

The results presented here suggest that the relationship between basin width, salt transport, and deep ventilation are complex. Meridional density differences are driven by density changes at both the north and south of the Atlantic basin (Fig. 10a) and also by changes in both temperature or salinity (Fig. 10b). This is in contrast to results in Jones and Cessi (2017), where salinity in the North Atlantic dominates destratification and deep-water formation. Moreover, while basin width certainly controls the barotropic circulation, the details by which the transport of salinity and temperature around the Atlantic basin and how that impacts the overturning circulation are not straightforward. In our simulations, the Wide Coast subpolar and subtropical gyre barotropic circulations are largest among the simulations (Table 2; Fig. 11). Both Coast's subpolar gyre is of similar strength to that of Straight Coast, but Both Coast has a much stronger subtropical gyre than Straight Coast, consistent with predicted increase in Sverdrup transport with basin width (Jones and Cessi 2017; Sverdrup 1947). However, Jones and Cessi's (2017) argument is not consistent with the larger MOC strength in Wide Coast as compared with Straight Coast.

While the MOC response to changes in basin shape is complicated, the MOC for each simulation is well predicted by the scaling derived by Butler et al. (2016). MOC scales with twice-integrated meridional density difference along the western coastline and with average basin width for ocean basins with both shaped and straight coasts. Moreover, the scaling is not sensitive to the choice of latitude for either the northern or the southern point for calculation of the meridional density difference. The density at only two locations in the ocean—one point at the north and one at the south of the basin—can provide a good estimate of MOC. Applying the Butler et al. (2016) scaling to several different continental configurations demonstrates the robustness of the scaling to different basin geometries that lead to large changes in MOC, despite the fact that the scaling was derived for a case with straight coastlines.

Salinity and temperature differences between simulations influence the stratification and meridional density gradient along the western boundary in the Atlantic-like basin, allowing the scaling developed by Butler et al. (2016) to accurately predict MOC strength. Causality in the relationship between meridional density gradient and MOC is difficult to ascribe due to the influence of remote Southern Ocean forcing on overturning (De Boer et al. 2010). Moreover, the meridional velocity is proportional to zonal pressure gradients, which are then related to meridional density differences through fast boundary waves (Johnson and Marshall 2002), so the relationship between meridional density gradient and MOC is not direct. Butler et al. (2016) posit that the MOC responds to the meridional density gradient through the creation of zonal pressure gradients or through ageostrophic flow. Thus, the differences in both temperature and salinity at the north and the south of the Atlantic-like basin across simulations act to cause meridional density gradient changes and in turn changes to MOC. The success of the Butler et al. (2016)

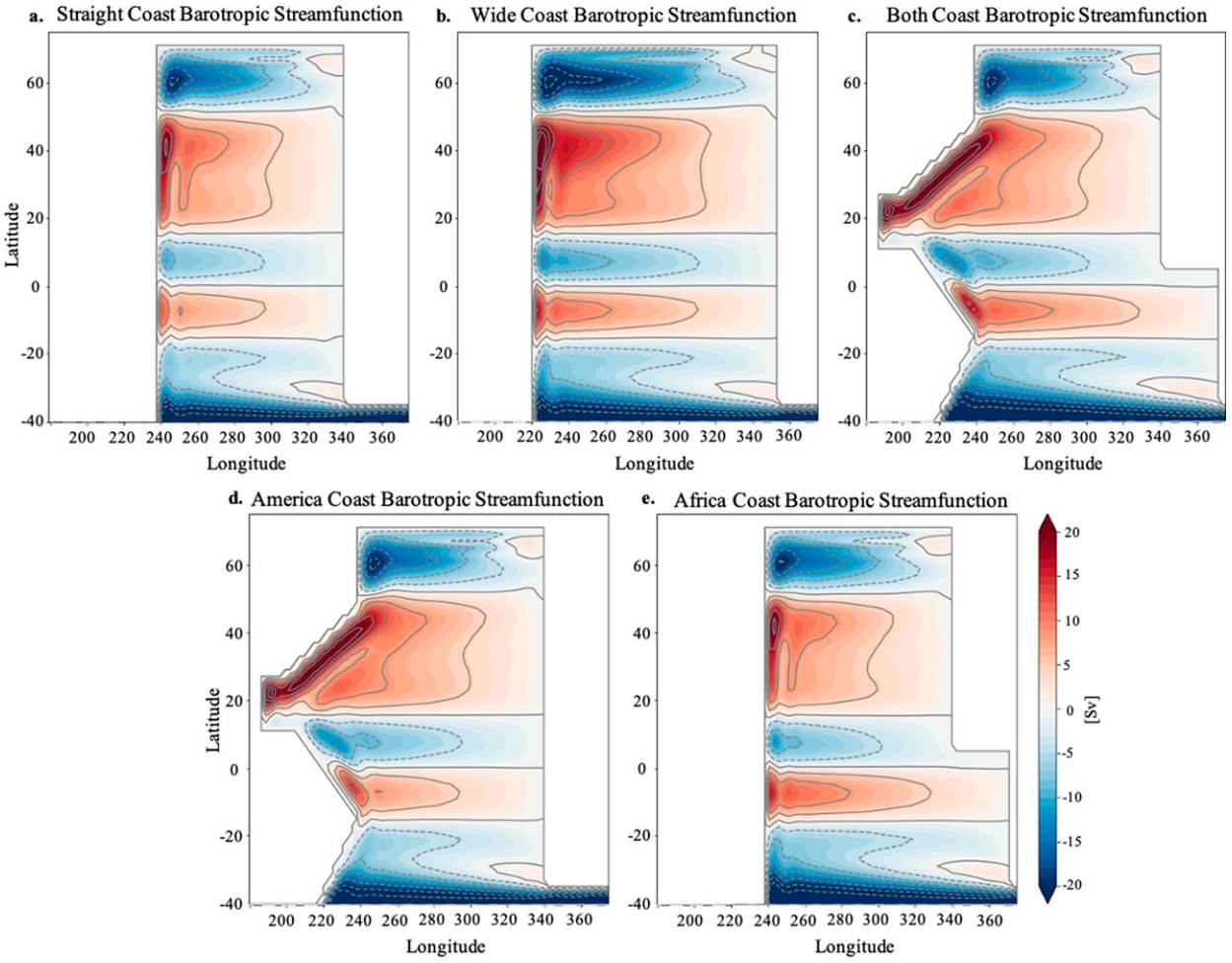

FIG. 11. The barotropic streamfunction for (a) Straight Coast, (b) Wide Coast, (c) Both Coast, (d) America Coast, and (e) Africa Coast. Red shading indicates clockwise circulation, and blue shading indicates counterclockwise circulation. Contours are every 5 Sv.

scaling demonstrates its versatility in reproducing MOC given density profiles at only two points in the Atlantic. While Butler et al. (2016) does not directly invoke the coupling of the barotropic circulation and the baroclinic structure of the gyres, inspection of the density difference between the surface and 1000 m (Fig. 7) and the barotropic circulation (Fig. 11) suggest that this coupling likely plays a large role in setting the density structure along the western boundary. This in turn suggests that basin geometry influences MOC through its influence on barotropic circulation.

Our model configurations represent a simplification of realistic continental configurations. However, they represent an increase in basin geometry complexity relative to past aquaplanet and other simulations with idealized continental configurations studies [such as Ferreira et al. (2010); Nilsson et al. (2013); Cessi and Jones (2017); Jones and Cessi (2017)]. As such, this study serves as an intermediate step in a hierarchy of ever more realistic idealized models aimed at better understanding the role of ocean basin geometry on ocean circulation. It is important to note that even the more realistically shaped coastlines in our model simulations are low-resolution simplifications of the real ocean boundaries. Also, by employing purely vertical, rather than sloping, ocean sidewalls and flat bottom bathymetry, we ignore the effects of topographically enhanced mixing and form drag as well as the role of bathymetry in steering abyssal flow. Despite these limitations, the continental configurations in this study demonstrate the importance of coastline shape on meridional overturning circulation and raise further questions about the role of interplay between meridional overturning and gyre transports for ocean stratification and circulation.

Acknowledgments. Authors Ragen, Armour, and Darr acknowledge support from National Science Foundation Award OCE-1850900. Author Shao was supported by MEOPAR and Grant IT15738 from MITACS. Author Thompson was supported by Grant NNX17AH56G as part of the NASA Ocean Surface Topography Science Team. We thank D. S. Battisti, A.

Gnanadesikan, E. A. Maroon, C. S. Jones, K. I. C. Oliver, R. C. J. Wills, and B. Green for helpful conversations and feedback on this project. Thanks also are given to two anonymous reviewers, whose comments greatly improved this work.

Data availability statement. Climatological data for this study are openly available on Zenodo (10.5281/zenodo.5544531).

REFERENCES

Adcroft, A., and Coauthors, 2019: The GFDL global ocean and sea ice model OM4.0: Model description and simulation features. *J. Adv. Model. Earth Syst.*, **11**, 3167–3211, https://doi.org/10.1029/2019MS001726.

Bell, M. J., 2015: Meridional overturning circulations driven by surface wind and buoyancy forcing. *J. Phys. Oceanogr.*, **45**, 2701–2714, https://doi.org/10.1175/JPO-D-14-0255.1.

Bryan, F., 1987: Parameter sensitivity of primitive equation ocean general circulation models. *J. Phys. Oceanogr.*, **17**, 970–985, https://doi.org/10.1175/1520-0485(1987)017<0970:PSOPEO>2.0.CO;2.

Buckley, M. W., and J. Marshall, 2016: Observations, inferences, and mechanisms of the Atlantic meridional overturning circulation: A review. *Rev. Geophys.*, **54**, 5–63, https://doi.org/10.1002/2015RG000493.

Butler, E., K. Oliver, J.-M. Hirschi, and J. Mecking, 2016: Reconstructing global overturning from meridional density gradients. *Climate Dyn.*, **46**, 2593–2610, https://doi.org/10.1007/s00382-015-2719-6.

Cessi, P., and C. Jones, 2017: Warm-route versus cold-route interbasin exchange in the meridional overturning circulation. *J. Phys. Oceanogr.*, **47**, 1981–1997, https://doi.org/10.1175/JPO-D-16-0249.1.

De Boer, A. M., A. Gnanadesikan, N. R. Edwards, and A. J. Watson, 2010: Meridional density gradients do not control the Atlantic overturning circulation. *J. Phys. Oceanogr.*, **40**, 368–380, https://doi.org/10.1175/2009JPO4200.1.

Delworth, T. L., and K. W. Dixon, 2006: Have anthropogenic aerosols delayed a greenhouse gas-induced weakening of the North Atlantic thermohaline circulation? *Geophys. Res. Lett.*, **33**, L02606, https://doi.org/10.1029/2005GL024980.

Drijfhout, S., G. J. Van Oldenborgh, and A. Cimatoribus, 2012: Is a decline of AMOC causing the warming hole above the North Atlantic in observed and modeled warming patterns? *J. Climate*, **25**, 8373–8379, https://doi.org/10.1175/JCLI-D-12-00490.1.

Fairall, C. W., E. F. Bradley, J. Hare, A. A. Grachev, and J. B. Edson, 2003: Bulk parameterization of air–sea fluxes: Updates and verification for the COARE algorithm. *J. Climate*, **16**, 571–591, https://doi.org/10.1175/1520-0442(2003)016<0571:BPOASF>2.0.CO;2.

Ferrari, R., and D. Ferreira, 2011: What processes drive the ocean heat transport? *Ocean Modell.*, **38**, 171–186, https://doi.org/10.1016/j.ocemod.2011.02.013.

Ferreira, D., J. Marshall, and J.-M. Campin, 2010: Localization of deep water formation: Role of atmospheric moisture transport and geometrical constraints on ocean circulation. *J. Climate*, **23**, 1456–1476, https://doi.org/10.1175/2009JCLI3197.1.

——, and Coauthors, 2018: Atlantic-Pacific asymmetry in deep water formation. *Annu. Rev. Earth Planet. Sci.*, **46**, 327–352, https://doi.org/10.1146/annurev-earth-082517-010045.

Frierson, D. M., and Coauthors, 2013: Contribution of ocean overturning circulation to tropical rainfall peak in the Northern Hemisphere. *Nat. Geosci.*, **6**, 940–944, https://doi.org/10.1038/ngeo1987.

Ganachaud, A., and C. Wunsch, 2000: Improved estimates of global ocean circulation, heat transport and mixing from hydrographic data. *Nature*, **408**, 453–457, https://doi.org/10.1038/35044048.

Gent, P. R., and J. C. McWilliams, 1990: Isopycnal mixing in ocean circulation models. *J. Phys. Oceanogr.*, **20**, 150–155, https://doi.org/10.1175/1520-0485(1990)020<0150:IMIOCM>2.0.CO;2.

Gnanadesikan, A., 1999: A simple predictive model for the structure of the oceanic pycnocline. *Science*, **283**, 2077–2079, https://doi.org/10.1126/science.283.5410.2077.

Griesel, A., and M. A. M. Maqueda, 2006: The relation of meridional pressure gradients to North Atlantic deep water volume transport in an ocean general circulation model. *Climate Dyn.*, **26**, 781–799, https://doi.org/10.1007/s00382-006-0122-z.

Jackson, L., R. Hallberg, and S. Legg, 2008: A parameterization of shear-driven turbulence for ocean climate models. *J. Phys. Oceanogr.*, **38**, 1033–1053, https://doi.org/10.1175/2007JPO3779.1.

Johnson, H. L., and D. P. Marshall, 2002: A theory for the surface Atlantic response to thermohaline variability. *J. Phys. Oceanogr.*, **32**, 1121–1132, https://doi.org/10.1175/1520-0485(2002)032<1121:ATFTSA>2.0.CO;2.

——, P. Cessi, D. P. Marshall, F. Schloesser, and M. A. Spall, 2019: Recent contributions of theory to our understanding of the Atlantic meridional overturning circulation. *J. Geophys. Res. Oceans*, **124**, 5376–5399, https://doi.org/10.1029/2019JC015330.

Jones, C. S., and P. Cessi, 2016: Interbasin transport of the meridional overturning circulation. *J. Phys. Oceanogr.*, **46**, 1157–1169, https://doi.org/10.1175/JPO-D-15-0197.1.

——, and ——, 2017: Size matters: Another reason why the Atlantic is saltier than the pacific. *J. Phys. Oceanogr.*, **47**, 2843–2859, https://doi.org/10.1175/JPO-D-17-0075.1.

Kaspi, Y., and T. Schneider, 2011: Winter cold of eastern continental boundaries induced by warm ocean waters. *Nature*, **471**, 621–624, https://doi.org/10.1038/nature09924.

Kostov, Y., K. C. Armour, and J. Marshall, 2014: Impact of the Atlantic meridional overturning circulation on ocean heat storage and transient climate change. *Geophys. Res. Lett.*, **41**, 2108–2116, https://doi.org/10.1002/2013GL058998.

Kuhlbrodt, T., A. Griesel, M. Montoya, A. Levermann, M. Hofmann, and S. Rahmstorf, 2007: On the driving processes of the Atlantic meridional overturning circulation. *Rev. Geophys.*, **45**, RG2001, https://doi.org/10.1029/2004RG000166.

Large, W., and S. Yeager, 2004: Diurnal to decadal global forcing for ocean and sea-ice models: The data sets and flux climatologies. NCAR Tech. Note NCAR/TN-460+STR, 105 pp., https://doi.org/10.5065/D6KK98Q6.

Lumpkin, R., and K. Speer, 2007: Global ocean meridional overturning. *J. Phys. Oceanogr.*, **37**, 2550–2562, https://doi.org/10.1175/JPO3130.1.

Marotzke, J., 1997: Boundary mixing and the dynamics of three-dimensional thermohaline circulations. *J. Phys. Oceanogr.*, **27**, 1713–1728, https://doi.org/10.1175/1520-0485(1997)027<1713:BMATDO>2.0.CO;2.

Marshall, J., and K. Speer, 2012: Closure of the meridional overturning circulation through Southern Ocean upwelling. *Nat. Geosci.*, **5**, 171–180, https://doi.org/10.1038/ngeo1391.

——, A. Donohoe, D. Ferreira, and D. McGee, 2014: The ocean's role in setting the mean position of the inter-tropical

convergence zone. *Climate Dyn.*, **42**, 1967–1979, https://doi.org/10.1007/s00382-013-1767-z.

Nilsson, J., G. Broström, and G. Walin, 2003: The thermohaline circulation and vertical mixing: Does weaker density stratification give stronger overturning? *J. Phys. Oceanogr.*, **33**, 2781–2795, https://doi.org/10.1175/1520-0485(2003)033<2781:TTCAVM>2.0.CO;2.

——, P. L. Langen, D. Ferreira, and J. Marshall, 2013: Ocean basin geometry and the salinification of the Atlantic Ocean. *J. Climate*, **26**, 6163–6184, https://doi.org/10.1175/JCLI-D-12-00358.1.

——, D. Ferreira, T. Schneider, and R. C. Wills, 2021: Is the surface salinity difference between the Atlantic and Indo-Pacific a signature of the Atlantic meridional overturning circulation? *J. Phys. Oceanogr.*, **51**, 769–787, https://doi.org/10.1175/JPO-D-20-0126.1.

Park, Y.-G., and K. Bryan, 2000: Comparison of thermally driven circulations from a depth-coordinate model and an isopycnal-layer model. Part I: Scaling-law sensitivity to vertical diffusivity. *J. Phys. Oceanogr.*, **30**, 590–605, https://doi.org/10.1175/1520-0485(2000)030<0590:COTDCF>2.0.CO;2.

Rahmstorf, S., 1996: On the freshwater forcing and transport of the Atlantic thermohaline circulation. *Climate Dyn.*, **12**, 799–811, https://doi.org/10.1007/s003820050144.

Reichl, B. G., and R. Hallberg, 2018: A simplified energetics based planetary boundary layer (ePBL) approach for ocean climate simulations. *Ocean Modell.*, **132**, 112–129, https://doi.org/10.1016/j.ocemod.2018.10.004.

Reid, J. L., Jr., 1961: On the temperature, salinity, and density differences between the Atlantic and Pacific oceans in the upper kilometre. *Deep-Sea Res.*, **7**, 265–275, https://doi.org/10.1016/0146-6313(61)90044-2.

Robinson, A., and H. Stommel, 1959: The oceanic thermocline and the associated thermohaline circulation 1. *Tellus*, **11**, 295–308, https://doi.org/10.3402/tellusa.v11i3.9317.

Rose, B. E., and J. Marshall, 2009: Ocean heat transport, sea ice, and multiple climate states: Insights from energy balance models. *J. Atmos. Sci.*, **66**, 2828–2843, https://doi.org/10.1175/2009JAS3039.1.

Sabine, C. L., and Coauthors, 2004: The oceanic sink for anthropogenic CO_2. *Science*, **305**, 367–371, https://doi.org/10.1126/science.1097403.

Schmittner, A., M. Latif, and B. Schneider, 2005: Model projections of the North Atlantic thermohaline circulation for the 21st century assessed by observations. *Geophys. Res. Lett.*, **32**, L23710, https://doi.org/10.1029/2005GL024368.

Shao, A. E., A. Adcroft, R. Hallberg, and S. M. Griffies, 2020: A general-coordinate, nonlocal neutral diffusion operator. *J. Adv. Model. Earth Syst.*, **12**, e2019MS001992, https://doi.org/10.1029/2019MS001992.

Sijp, W. P., and M. H. England, 2009: Southern Hemisphere westerly wind control over the ocean's thermohaline circulation. *J. Climate*, **22**, 1277–1286, https://doi.org/10.1175/2008JCLI2310.1.

——, J. M. Gregory, R. Tailleux, and P. Spence, 2012: The key role of the western boundary in linking the AMOC strength to the north–south pressure gradient. *J. Phys. Oceanogr.*, **42**, 628–643, https://doi.org/10.1175/JPO-D-11-0113.1.

Smethie, W. M., Jr., and R. A. Fine, 2001: Rates of North Atlantic deep water formation calculated from chlorofluorocarbon inventories. *Deep-Sea Res. I*, **48**, 189–215, https://doi.org/10.1016/S0967-0637(00)00048-0.

Stommel, H., 1961: Thermohaline convection with two stable regimes of flow. *Tellus*, **13**, 224–230, https://doi.org/10.3402/tellusa.v13i2.9491.

Straneo, F., 2006: On the connection between dense water formation, overturning, and poleward heat transport in a convective basin. *J. Phys. Oceanogr.*, **36**, 1822–1840, https://doi.org/10.1175/JPO2932.1.

Sun, S., A. F. Thompson, and I. Eisenman, 2020: Transient overturning compensation between Atlantic and Indo-Pacific basins. *J. Phys. Oceanogr.*, **50**, 2151–2172, https://doi.org/10.1175/JPO-D-20-0060.1.

Sutton, R. T., and D. L. Hodson, 2005: Atlantic Ocean forcing of North American and European summer climate. *Science*, **309**, 115–118, https://doi.org/10.1126/science.1109496.

Sverdrup, H. U., 1947: Wind-driven currents in a baroclinic ocean; with application to the equatorial currents of the eastern Pacific. *Proc. Natl. Acad. Sci. USA*, **33**, 318–326, https://doi.org/10.1073/pnas.33.11.318.

Talley, L. D., 2003: Shallow, intermediate, and deep overturning components of the global heat budget. *J. Phys. Oceanogr.*, **33**, 530–560, https://doi.org/10.1175/1520-0485(2003)033<0530:SIADOC>2.0.CO;2.

——, 2008: Freshwater transport estimates and the global overturning circulation: Shallow, deep and throughflow components. *Prog. Oceanogr.*, **78**, 257–303, https://doi.org/10.1016/j.pocean.2008.05.001.

Thorpe, R., J. M. Gregory, T. Johns, R. Wood, and J. Mitchell, 2001: Mechanisms determining the Atlantic thermohaline circulation response to greenhouse gas forcing in a non-flux-adjusted coupled climate model. *J. Climate*, **14**, 3102–3116, https://doi.org/10.1175/1520-0442(2001)014<3102:MDTATC>2.0.CO;2.

Trenberth, K. E., and J. M. Caron, 2001: Estimates of meridional atmosphere and ocean heat transports. *J. Climate*, **14**, 3433–3443, https://doi.org/10.1175/1520-0442(2001)014<3433:EOMAAO>2.0.CO;2.

Vellinga, M., and R. A. Wood, 2002: Global climatic impacts of a collapse of the Atlantic thermohaline circulation. *Climatic Change*, **54**, 251–267, https://doi.org/10.1023/A:1016168827653.

Wang, X., P. H. Stone, and J. Marotzke, 1995: Poleward heat transport in a barotropic ocean model. *J. Phys. Oceanogr.*, **25**, 256–265, https://doi.org/10.1175/1520-0485(1995)025<0256:PHTIAB>2.0.CO;2.

Warren, B. A., 1983: Why is no deep water formed in the North Pacific? *J. Mar. Res.*, **41**, 327–347, https://doi.org/10.1357/002224083788520207.

Watson, A. J., G. K. Vallis, and M. Nikurashin, 2015: Southern Ocean buoyancy forcing of ocean ventilation and glacial atmospheric CO_2. *Nat. Geosci.*, **8**, 861–864, https://doi.org/10.1038/ngeo2538.

Winton, M., S. M. Griffies, B. L. Samuels, J. L. Sarmiento, and T. L. Frölicher, 2013: Connecting changing ocean circulation with changing climate. *J. Climate*, **26**, 2268–2278, https://doi.org/10.1175/JCLI-D-12-00296.1.

Wolfe, C. L., and P. Cessi, 2010: What sets the strength of the middepth stratification and overturning circulation in eddying ocean models? *J. Phys. Oceanogr.*, **40**, 1520–1538, https://doi.org/10.1175/2010JPO4393.1.

Woollings, T., J. M. Gregory, J. G. Pinto, M. Reyers, and D. J. Brayshaw, 2012: Response of the North Atlantic storm track to climate change shaped by ocean–atmosphere coupling. *Nat. Geosci.*, **5**, 313–317, https://doi.org/10.1038/ngeo1438.

Wright, D. G., 1997: An equation of state for use in ocean models: Eckart's formula revisited. *J. Atmos. Oceanic Technol.*, **14**, 735–740, https://doi.org/10.1175/1520-0426(1997)014<0735:AEOSFU>2.0.CO;2.

Youngs, M. K., R. Ferrari, and G. R. Flierl, 2020: Basin-width dependence of northern deep convection. *Geophys. Res. Lett.*, **47**, e2020GL089135, https://doi.org/10.1029/2020GL089135.